

CHAPTER III

EXPLOSIVE ENVIRONMENTS

3.1 INTRODUCTION

General airblast phenomenology is presented in this chapter along with a discussion of TNT equivalency, blast scaling, the process of venting through the perforated walls of suppressive structures, and external airblast properties. Prediction methods are presented which allow a designer to estimate internal blast loads on suppressive shields or other types of containment structures. Methods are given for predicting both the initial reflected shock loading and the later relatively long term gas venting overpressure which can significantly load structures with small or no venting.

Prediction of fragment effects is divided into definition of fragment threat and to penetration of fragments. Both primary and secondary fragments are considered. A general discussion of fireball and thermal effects including attenuation by suppressive structures is given next. No prediction methods for thermal effects have been included because of insufficient data.

3.2 BLAST WAVES IN AIR

3.2.1 General

Blast wave formation and transmission through air have been studied extensively over the last 60 years, so the general characteristics of these waves are relatively well known and documented (see, e.g., Ref. 3-1). Airblast waves of interest in suppressive shielding are typically the result of an explosion. The word explosion as used in this handbook implies a process by which a pressure wave of finite amplitude is generated in air by a rapid release of energy. The energy source

will be, almost without exception, a compact quantity of chemical materials insofar as this handbook is concerned. Regardless of the source of the initial finite pressure disturbance, the properties of air as a compressible gas will cause the front of this disturbance to steepen as it passes through the air until it exhibits nearly discontinuous increases in pressure, density, and temperature. The resulting shock front moves supersonically. The air particles are also accelerated by the passage of the shock front, producing a net particle velocity in the direction of travel of the front.

If it is assumed that an explosion occurs in a still, homogeneous atmosphere and that the source is spherically symmetric, the characteristics of the blast wave are functions only of the properties of the explosive, the distance R from the center of the source and the time t . Let it be assumed that an ideal pressure transducer, which offers no resistance to flow behind the shock front and follows perfectly all variations in pressure, is used to record the time history of incident overpressure at some given fixed distance R from the explosion. The record that such a gage would produce is shown in Fig. 3-1. When the shock front arrives at arrival time t_a , the pressure rises quite abruptly to a peak value P_{so} . The pressure then decays to ambient in a time t_o , drops to a partial vacuum of amplitude P_{so}^- , and eventually returns to ambient in total time $t_a + t_o + t_o^-$. The quantity P_{so} is termed the peak side-on overpressure, as opposed to reflected overpressure.

The portion of the time-history curve above ambient pressure is called the positive phase. That portion of the time-history below ambient pressure is called the negative phase. The areas under these curves define the airblast wave incident positive and negative impulse, respectively. The negative phase of the blast wave is not important in the design and analysis of suppressive shields and will not be treated in this handbook.

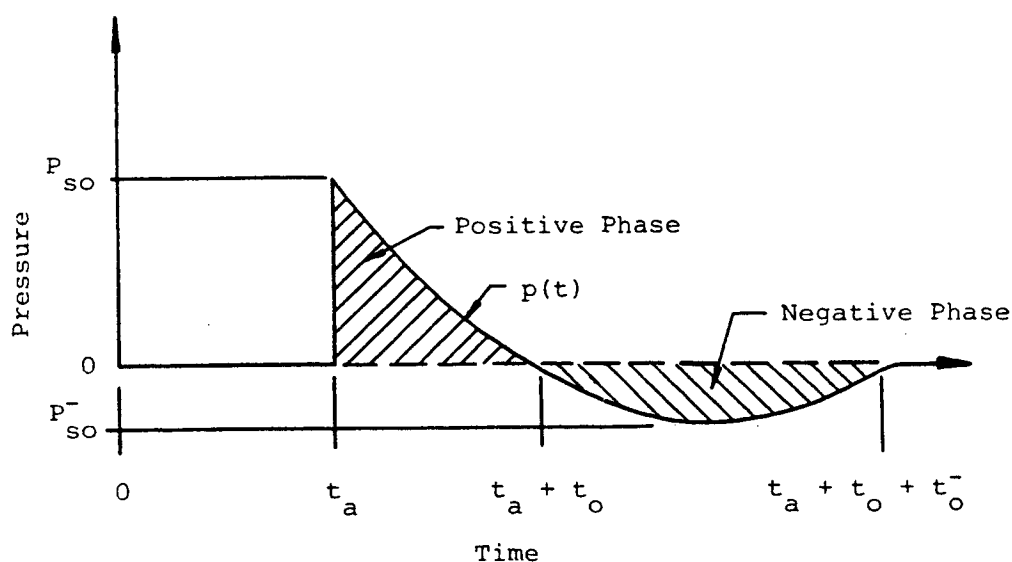


Figure 3-1. Ideal Blast Wave

The airblast wave depicted in Fig. 3-1 is a free-field phenomenon, i.e., the blast wave as it would appear over an ideal surface and under ideal conditions. Upon encountering any solid or dense object, the free-field blast waves are seriously modified as they reflect from and diffract around the object. These processes are of more interest in the external airblast loading of structures than in suppressive shielding and are covered in some detail in Refs. 3-2 and 3-3. Reflected airblast, which is of primary interest in suppressive shielding, will be covered in a later paragraph on internal airblast.

3.2.2 TNT Equivalence

The standard explosive for determination of blast effects in this handbook will be TNT. Other chemical explosives generate airblast waves which differ somewhat in their characteristics from TNT. The general wave characteristics are quite similar, but detailed properties such as peak pressure and impulse are measurably different for identical charge weights. Conversion of other types of explosive to their TNT equivalent, e_t , can be accomplished on the basis of charge weight, i.e.,

$$W_{\text{TNT}} = e_t \times W \quad (3-1)$$

where

W_{TNT} = equivalent charge weight of TNT, lb

e_t = factor from Table 3-1

W = explosive of interest charge weight, lb

The TNT equivalence factors listed in Table 3-1 have been developed by ratio of relative heats of explosion (Refs. 3-1 and 3-4). These factors are best average values and are recommended for suppressive shields only. They take into consideration the need for data on quasi-static pressure as well as blast impulse and related overpressures. For close-in explosions ($Z < 3.0 \text{ ft/lb}^{1/3}$) and for shapes of explosives other than spheres, the TNT equivalence factors can be much greater than those obtained from relative heats of explosion. Much work has been done on determination of TNT equivalency for specific compositions, distances, and shapes. References 3-5 through 3-14 are typical examples of these types of data.

Determination of airblast effects for use with the methods presented in this handbook, then, will be on the basis of an equivalent charge weight of TNT established in accordance with Eq. 3-1.

3.2.3 Scaling

A number of blast scaling laws have been proposed, (see, e.g., Ref. 3-1), but by far the most widely accepted are the Hopkinson-Cranz and Sachs laws. These two laws have been very well verified by experiment. The Hopkinson-Cranz law was formulated independently by B. Hopkinson in England and by C. Cranz in Germany during World War I. It allows prediction of blast wave properties from small scale experiments for any other scale, over all corresponding scaled distances, provided the type of explosive source, the geometry of the source and the

Table 3-1
TNT EQUIVALENCE FACTORS FOR
CHEMICAL EXPLOSIVES

Explosive	e_t (TNT Equivalent)
Amatol 60/40 (60% ammonium nitrate, 40% TNT)	0.586
Baronal (50% barium nitrate, 35% TNT, 15% aluminum)	1.051
Comp B (60% RDX, 40% TNT)	1.148
C-4 (91% RDX, 9% plasticizer)	1.078
Explosive D (ammonium picrate)	0.740
H-6 (45% RDX, 30% TNT, 20% Al, 5% D-2 wax)	0.854
HBX-1 (40% RDX, 38% TNT, 17% Al, 5% D-2 wax)	0.851
HMX	1.256
Lead Azide	0.340
Lead Styphnate	0.423
Mercury Fulminate	0.395
Nitroglycerine (liquid)	1.481
Nitroguanidine	0.668
Octol, 70/30 (70% HMX, 30% TNT)	0.994
PETN	1.282
Pentolite, 50/50 (50% PETN, 50% TNT)	1.129
Picric Acid	0.926
RDX (Cyclonite)	1.185
Silver Azide	0.419
Tetryl	1.00
TNT	1.00
Torpex (42% RDX, 40% TNT, 18% Al)	1.667
Tritonal (80% TNT, 20% Al)	1.639

(Refs. 3-1 and 3-4)

experiment are identical. Sachs scaling, formulated by R. G. Sachs during World War II, allows prediction of the effects of detonations in different atmospheric conditions. It is unlikely that suppressive shields will be located at high enough altitudes for ambient atmospheric conditions to be significantly different from conditions at sea level; therefore, Sachs scaling is not included in this handbook.

The Hopkinson-Cranz law states that self-similar blast (shock) waves are produced at identical scaled distances when two explosive charges of similar geometry and the same explosive composition, but of different size, are detonated in the same atmosphere. The customary scaled distance Z is defined as

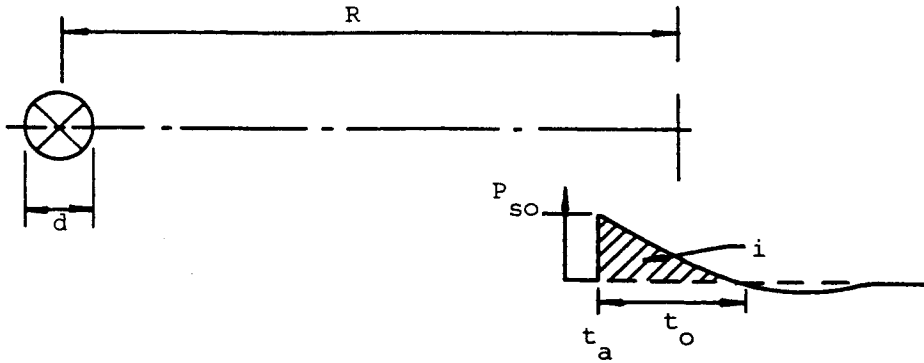
$$Z = R/W^{1/3} \quad (3-2)$$

where

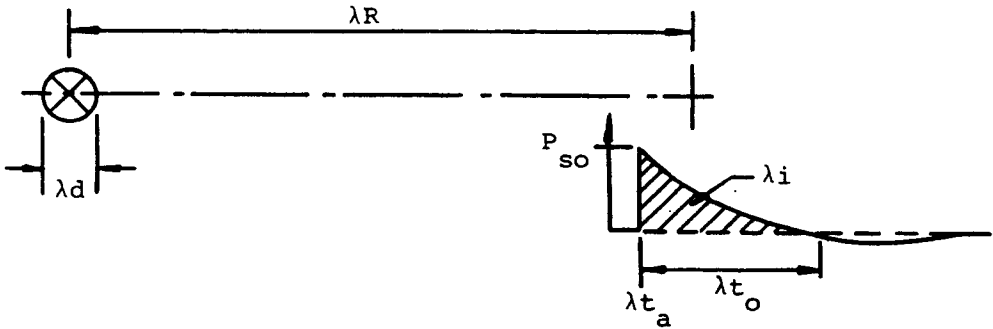
R = distance from the center of the explosive source to the point of interest, ft

W = explosive charge weight, lb

Scaling of airblast parameters is illustrated in Fig. 3-2. An observer located a distance R from the center of an explosive source of characteristic dimension d will be subjected to a blast wave with an amplitude (peak overpressure) P_{so} , a duration t_o , and a characteristic pressure-time history $p(t)$. The positive impulse i in the blast wave is defined as the area under the positive phase of the airblast pressure-time history curve. The Hopkinson-Cranz scaling law states that an observer stationed a distance λR from the center of a similar explosive source of characteristic dimension λd detonated in the same atmosphere will feel a blast wave of a similar form, the same amplitude P_{so} , but a duration λt_o and impulse λi . All characteristic times, such as arrival time t_a , are scaled by the same factor as the length scale factor λ . In Hopkinson-Cranz scaling, pressures and velocities are the same at scaled distances at scaled times.



a. Full Size Experiment



b. Scaled Experiment

Figure 3-2. Hopkinson-Cranz Scaling of Airblast Parameters

The Hopkinson-Cranz scaling law has become so universally used that chemical explosive blast data are almost always presented in terms of Hopkinson-Cranz scaled parameters. That is, pressures, times and impulses, both incident and reflected, can be conveniently presented as unique functions of the scaled distance Z .

3.2.4 Prediction of Free-Field Airblast Parameters

There are a number of data sources for scaled blast parameters. References 3-1 and 3-4 give shock front properties for incident and normally reflected waves, as well as scaled times and impulses, for spherical Pentolite charges detonated

in free air (far from any reflecting surface). Data are given in Ref. 3-15 for incident waves from surface bursts of TNT which are generally accepted as the standard curves for this reflection situation. References 3-2, 3-16 and 3-17 contain compilations for both free-air and surface bursts of TNT.

If properly used, all of these references will give predictions of blast wave properties which are reasonably close to each other (with the possible exception of durations, t_o), although not all cover identical ranges of scaled distance. Free-field, or incident, blast wave properties which are important in the loading of suppressive shields are presented in Fig. 3-3. These parameters include P_{so} , i_s , t_a and t_o . Reflected airblast parameters are presented in a later paragraph on internal blast in this handbook. All parameters are scaled according to the Hopkinson-Cranz law, using in-lb-sec units, and data are presented for spherical TNT charges in free air. Standard sea level atmospheric conditions are assumed (ambient pressure $P_o = 14.696$ psi and sound speed $a_o = 1117$ ft/sec).

These curves can be used to estimate data for surface bursts by using an effective charge weight which accounts for ground reflection. The suggested conversion is

$$W_e = 1.8 W \quad (3-3)$$

where W_e is the effective charge weight in pounds of TNT to be used for estimating surface burst effects with the free air charts presented herein. This conversion has been shown to give good agreement with the data reported in Ref. 3-15.

It is sometimes necessary to estimate the velocity U at which the shock front of an airblast wave is traveling. The shock front velocity is a function of the peak overpressure and can be found from Fig. 3-4.

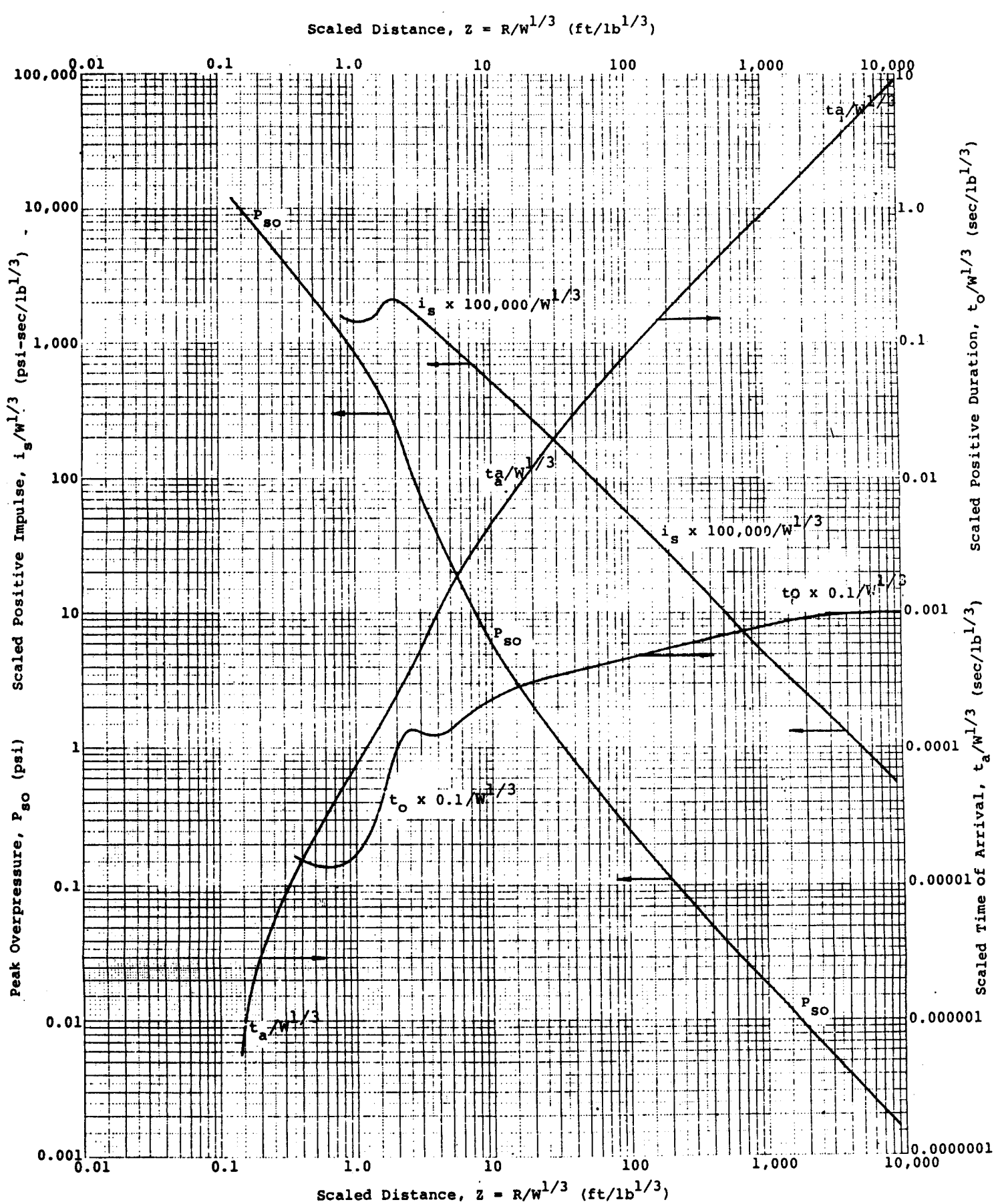


Figure 3-3. Incident Airblast Parameters for Spherical TNT Free Air Burst
(Southwest Research Institute)

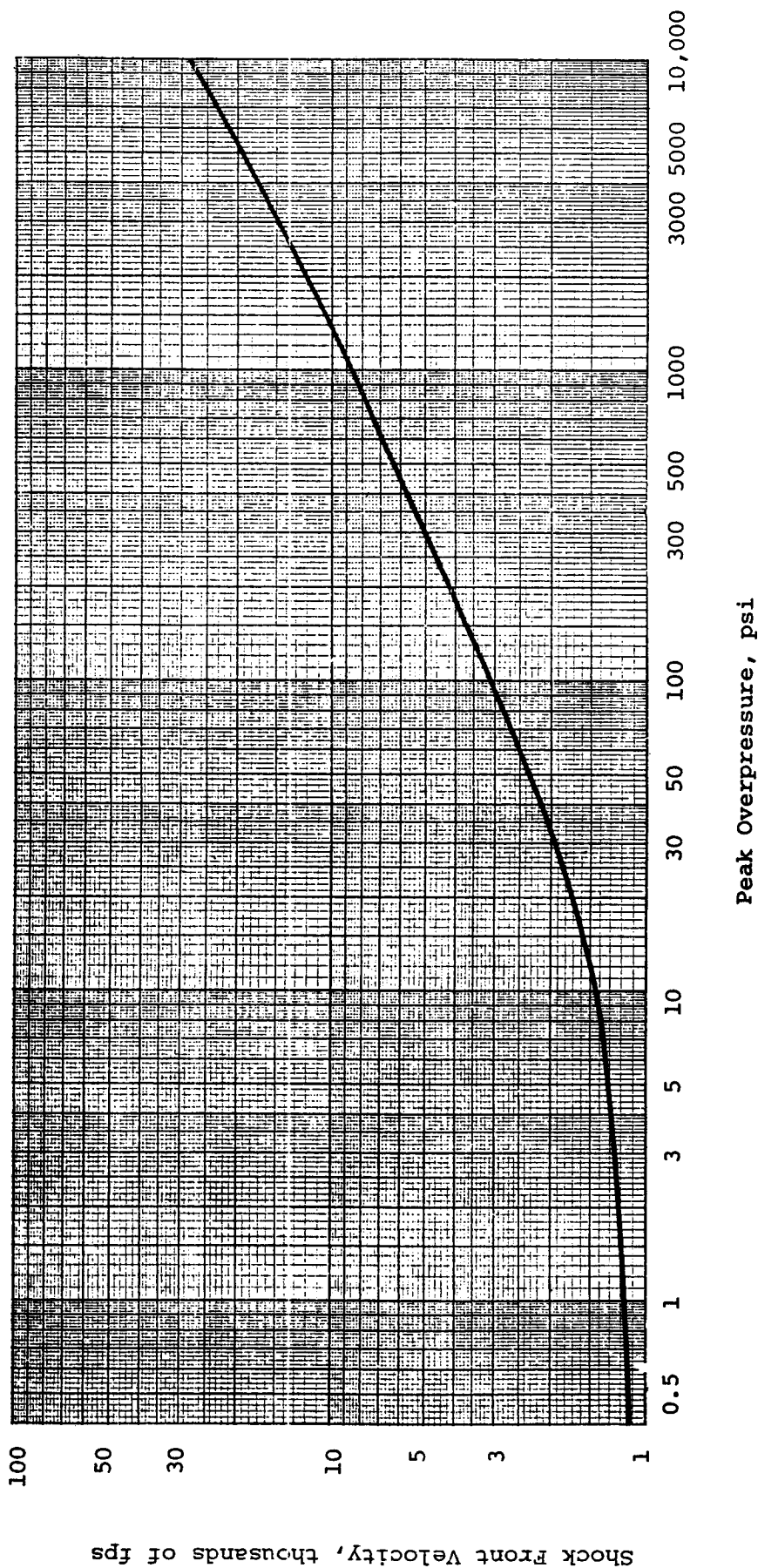


Figure 3-4. Shock Front Velocity as a Function of Peak Overpressure at Sea Level
(Ref. 3-3)

3.3 INTERNAL AIRBLAST

3.3.1 General

The loading from an explosive charge detonated within a vented or unvented structure consists of two almost distinct phases. The first phase is the reflected blast loading, which consists of an initial high pressure, short duration reflected wave, plus perhaps several later reflected pulses arriving at times closely approximated by twice the average first pulse arrival time at the chamber walls. These later pulses are usually attenuated in amplitude because of irreversible thermodynamic processes and are very complex in waveform because of the nature of the reflection process within the structure, whether vented or unvented. The second loading phase is a quasi-static pressure pulse and is discussed in a following paragraph.

The simplest case of blast wave reflection is that of normal reflection of a plane shock wave from a plane, rigid surface. In this case, the incident wave moves at velocity U through still air at ambient conditions. The conditions immediately behind the shock front are those for the free air shock wave discussed above. When the incident shock wave strikes the plane rigid surface, it is reflected therefrom. The reflected wave now moves away from the surface with a velocity U_r into the flow field and compressed region associated with the incident wave. In the reflection process, the incident particle velocity u_s is arrested ($u_s = 0$ at the reflecting surface), and the pressure, density, and temperature of the reflected wave are all increased above the values in the incident wave. The overpressure at the wall surface is termed the reflected overpressure and is designated P_r . For very weak shocks, $P_{so} \ll P_o$, acoustic approximations are valid, and the reflected overpressure is twice the incident overpressure, $P_r = 2P_{so}$. For stronger incident shocks, the enhancement of reflected pressure is increased by a factor of up to eight or more.

The durations of normally reflected waves are assumed to be not greatly different from those of incident waves. Reflected overpressures, however, are much higher than incident overpressures with the result that the reflected impulses are much greater than the incident impulses.

Following the initial shock wave reflection from the internal walls of a suppressive shield, the internal blast pressure loading becomes quite complex in nature. Figure 3-5 shows a stage in the loading for the cylindrical Group 3 suppressive shield. At the instant shown, portions of the cap, base and cylindrical surface are loaded by the reflected shock and the incident shock is reflecting obliquely from all three internal surfaces. The oblique reflection process can generate Mach waves (see Ref. 3-1 for a description of Mach waves), if the angle of incidence is great enough and pressures can be greatly enhanced on entering corners or reflecting near the axis of a cylindrical structure. In box-shaped suppressive shields, the reflection process can be even more complex.

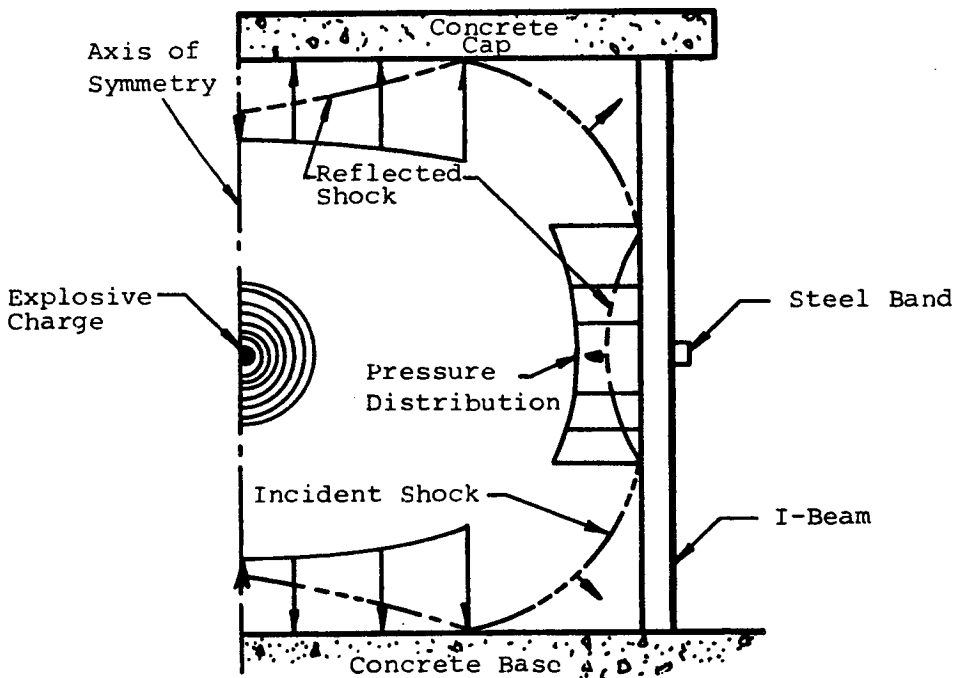


Figure 3-5. Schematic Representation of Shock Reflections from Interior Walls of a Suppressive Shield (Ref. 3-18)

Following the initial internal blast loading, the shock waves reflected inward will tend to strengthen as they implode toward the center of the structure and then re-reflect to load the structure again. As noted earlier, each of these later shocks will usually be less severe than the preceding shock. After several such reflections, which occur in a very short time, the initial internal blast phase of the loading is over.

3.3.2 Prediction of Internal Blast Loads

The air shock loading on the interior surfaces of suppressive shields is quite complex for all real structural geometries. Fortunately, however, approximate loading predictions suitable for the purposes of this handbook can be made with the aid of various simplifying assumptions. First, it is assumed that the initial reflected airblast parameters can be taken as the ideal normally reflected parameters, even for oblique reflections from the structure walls. This assumption is almost exactly true for strong shock waves up to an angle of incidence of about 40 degrees and for weak shock waves up to about 70 degrees, provided the slant range from the center of the charge to the point of interest is used for R in Eq. 3-2, pg. 3-6. Since most suppressive shield designs are reasonably symmetrical with length-to-height and width-to-height ratios of near one, and because well-designed suppressive shields will have the charge essentially centrally located, shock reflections from the walls will be fairly regular almost everywhere.

Ideal normally reflected blast parameters for a free air burst of spherical TNT are presented in Fig. 3-6. The time of duration of the initial reflected pulse is taken as

$$t_r = 2i_r/P_r \quad (3-4)$$

The re-reflected aftershocks are neglected in the simplified structural response methods presented in this handbook; therefore, the reflected impulse (i_r) and peak reflected pressure (P_r)

Scaled Distance, $Z = R/W^{1/3}$ (ft/lb^{1/3})

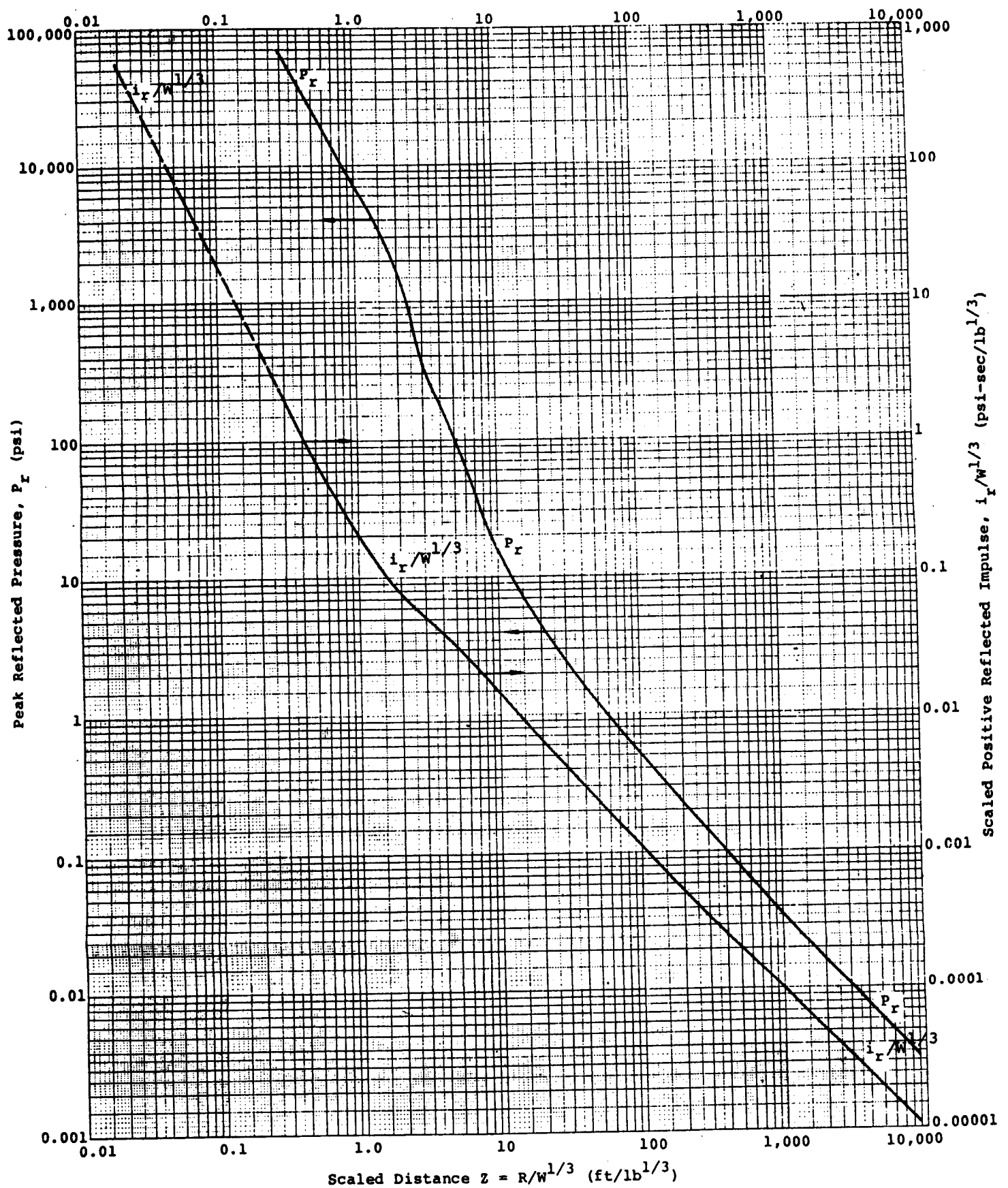


Figure 3-6. Reflected Airblast Parameters for Spherical TNT Free Air Burst
(Southwest Research Institute)

are the only initial internal blast parameters needed. For more exact calculations of loading, arrival times of the shock front and re-reflected aftershocks as a function of position in the structure can be important and should be considered.

3.4 VENTING

3.4.1 Introduction

The discussion of airblast loading up to this point has been largely in terms of solid containment vessels, i.e., structures with no venting. The desired function of a suppressive shield is to reduce the effects of an accidental explosion to an acceptable level as economically as possible. An optimum amount of venting can contribute materially to meeting this objective. Venting is essential for suppressive shields designed for containment of deflagrating materials (e.g., Shield Group 5); otherwise, the deflagration can escalate to a detonation if the gaseous products are not dissipated at an adequate rate.

3.4.2 Vent Area Ratio

The vent area ratio for a single layer structure is the vent area divided by the total area of the wall. The vent area ratio for a multi-layer structure proposed in Ref. 3-19 is

$$\frac{1}{\alpha_e} = \sum_{i=1}^n \frac{1}{\alpha_i} \quad (3-5)$$

where α_e is the multi-layer and α_i is the single layer vent area ratio for an n-layer structure.

The vent area ratio for a perforated plate is simply

$$\alpha_i = A_{vi}/A_{wi} \quad (3-6)$$

where A_{vi} and A_{wi} are the vent area and wall area of the i th layer, respectively. For cubicles with a portion or all of a wall or roof missing, the vent area is the area of the opening

and the appropriate value for α_e is the ratio of the open area to the total interior area of the cubicle.

Procedures for calculating vent area ratios for various structural configurations which have been used for suppressive shields are presented in Fig. 3-7. The procedures shown in Fig. 3-7, which are developed in Ref. 3-19, are believed to be self-explanatory, except possibly for the interlocked I-beams. The vent areas number 2 and 3 for this case are to take account of the two equal spaces b associated with each I-beam.

3.5 QUASI-STATIC PRESSURES

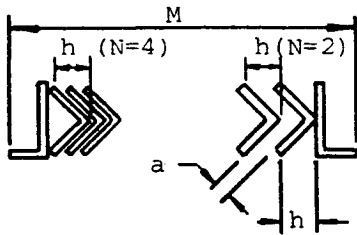
3.5.1 General

When an explosion occurs within a suppressive structure, the overpressure eventually settles to a slowly decaying level, which is a function of the volume and vent area of the structure and the nature and energy release of the explosion. A typical time history of overpressure at the wall of a suppressive structure is shown in Fig. 3-8a. The typical actual time history shown in Fig. 3-8a is idealized to the two triangle pulse depicted in Fig. 3-8b for use with the simplified structural response methods of this handbook.

Determination of the short duration initial impulsive portion of the idealized loading function has been addressed in paragraph 3.3 above. Prediction of the idealized long duration quasi-static portion of the loading is presented below.

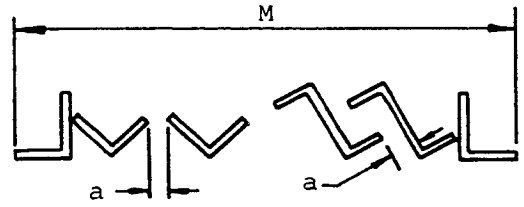
3.5.2 Prediction of Quasi-Static Pressure Parameters

The two parameters of interest for construction of the quasi-static portion of the idealized loading function are the peak quasi-static pressure, P_{qs} , and the time, t_b , at which the quasi-static pressure returns to ambient. This time to return to ambient pressure is often referred to as the blowdown time.



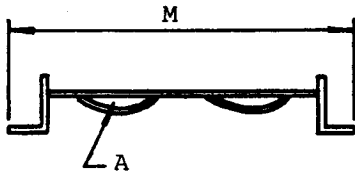
$A_v = nla/N$
 n = number of openings
 l = length of exposed element
 h = projected width of angle
 N = 2 for one opening per projected width h of angle; = 4 for two or more openings per width h
 $A_w = LM$
 L = length of wall
 $\alpha_i = A_v/A_w$
 M = panel width

(a) Nested Angles



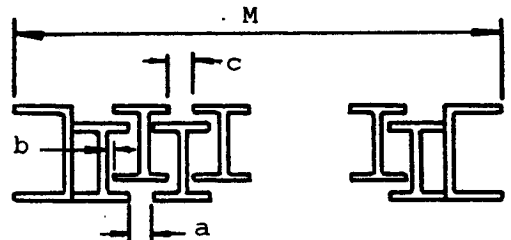
$A_v = nla$
 n = number of openings
 l = length of exposed element
 $A_w = LM$
 L = length of wall
 $\alpha_i = A_v/A_w$
 M = panel width

(b) Side-by-Side Angles or Zees



$A_v = nA/2$
 n = number of louvres
 A = open area of louvre
 $A_w = LM$
 L = Length of wall
 $\alpha_i = A_v/A_w$
 M = panel width

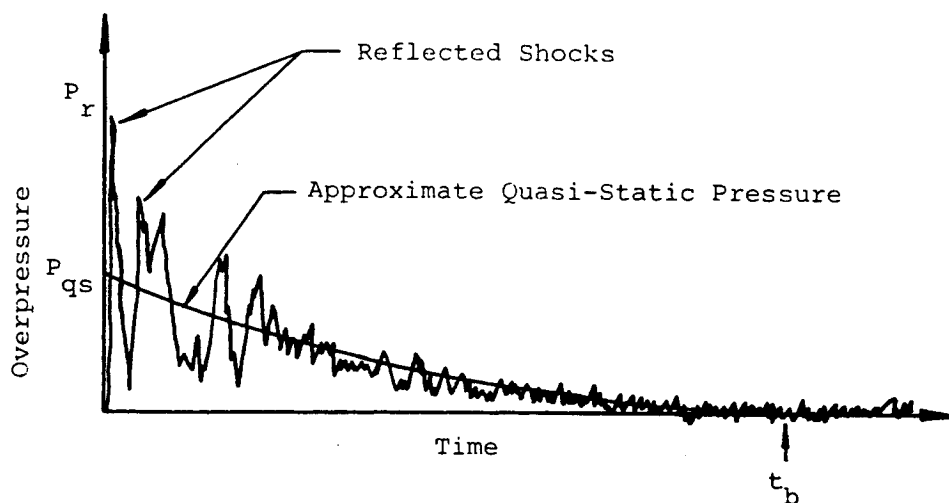
(c) Louvres



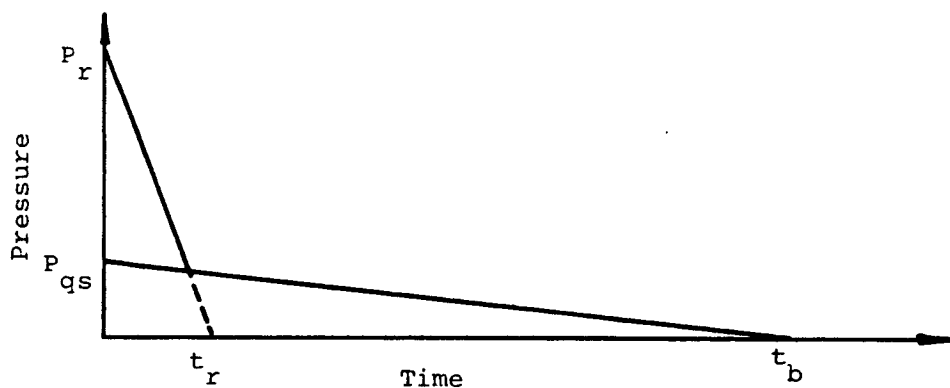
M = panel width
 $A_{v1} = 2ln_a a$
 $A_{v2} = A_{v3} = 2ln_b b$
 $A_{v4} = 2ln_c c$
 n_a, n_b, n_c = number of openings a, b, c
 l = length of element
 $A_w = LM$
 L = length of wall
 $\alpha_1 = A_{v1}/A_w, \alpha_2 = A_{v2}/A_w, \dots$

(d) Interlocked I-Beams

Figure 3-7. Definition of Vent Area Ratios for Various Structural Configurations (Ref. 3-19)



a. Typical Actual Pressure-Time History (Electronically Filtered)



b. Idealized Pressure-Time History

Figure 3-8. Internal Pressure Loading at Inner Surface of a Suppressive Shield

The maximum value for the quasi-static pressure in the long duration phase of the loading is the pressure rise which would occur in an unvented enclosure before heat transfer effects attenuate it. From data and analyses reported in Refs. 3-19 through 3-25, the curve of Fig. 3-9 has been shown to yield good predictions of P_{qs} as a function of the charge to volume ratio W/V . The charge weight W in Fig. 3-9 is in pounds of TNT and the internal volume, V , of the structure is in cubic feet.

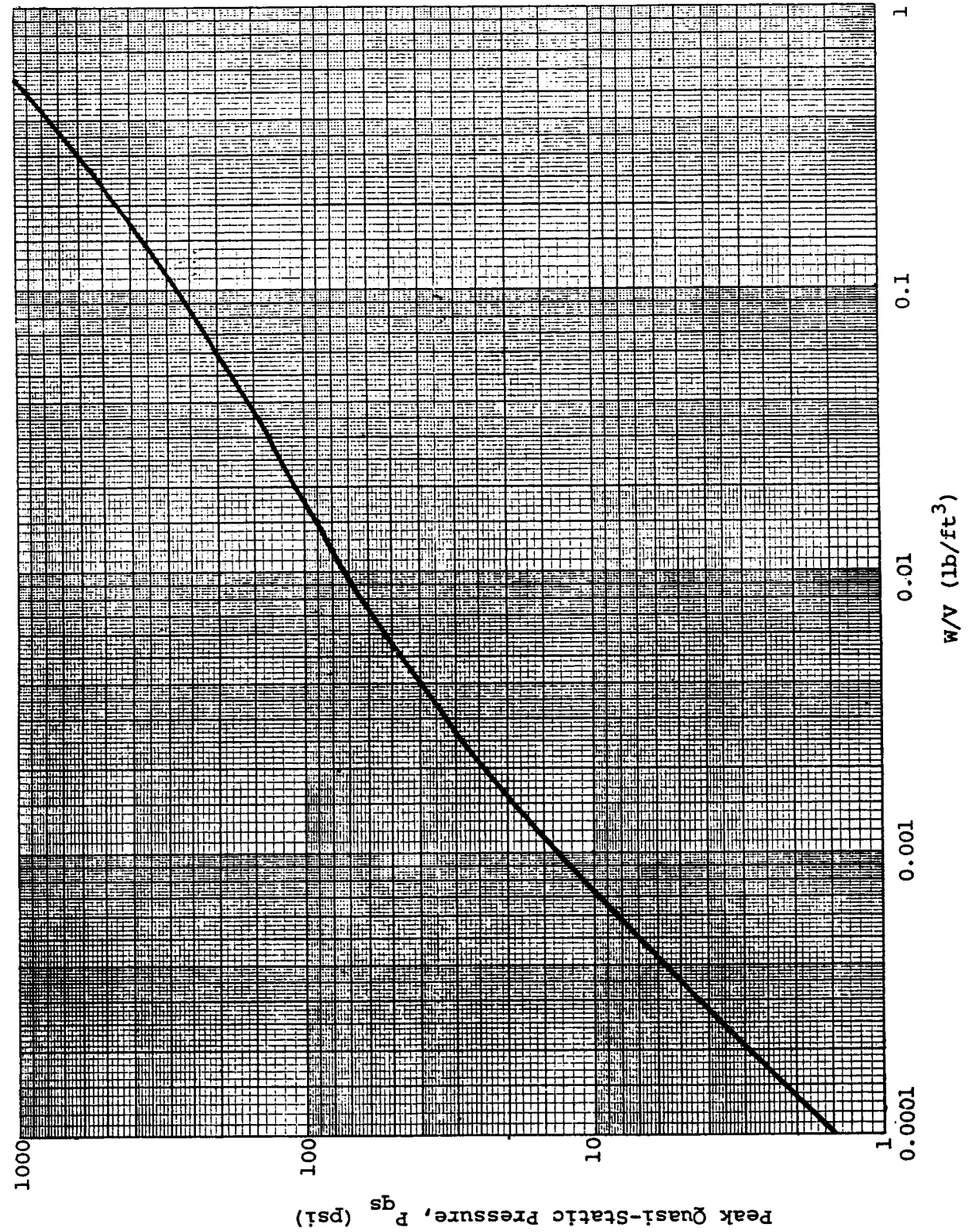


Figure 3-9. Peak Quasi-Static Pressure
(Southwest Research Institute)

The blowdown time, t_b , can be determined with Fig. 3-10 once P_{qs} has been established. In using Fig. 3-10,

P_o = ambient pressure, psi

a_o = speed of sound, 1117 ft/sec

V = internal volume of suppressive shield, ft^3

A_i = internal vented surface area of suppressive shield, ft^2

α_e = vent area ratio, Eq. 3-5, pg. 3-17

The internal vented surface area is the total surface area of those surfaces which are vented. For example, if the side walls are vented, but the roof and floor are not, A_i is equal to the total interior surface area of the walls, i.e., the roof and floor areas are not included.

3.6 AIRBLAST OUTSIDE SUPPRESSIVE SHIELDS

3.6.1 General

Most of the suppressive shield group designs have walls, or walls and roof, which have been designed to provide uniform venting. The vented wall/roof panel designs, which are discussed in more detail in Appendix A, consist of various combinations of perforated plates, nested angles or zees, louvres, and interlocked I-beams.

As each incident shock wave strikes the inner surface of a vented panel in a suppressive structure as shown in Fig. 3-11(a), it is partially reflected and partially transmitted undiminished in strength into the holes or slits in the first layer of the panel. The influence of viscosity is seen as a build-up of vortices at the entrance; see Fig. 3-11(a). At a later time, this vortex becomes detached and is swept into the restriction, forming a contraction (vena contracta) as shown in Figs. 3-11(b) through (d). The transmitted wave emerges from the restriction,

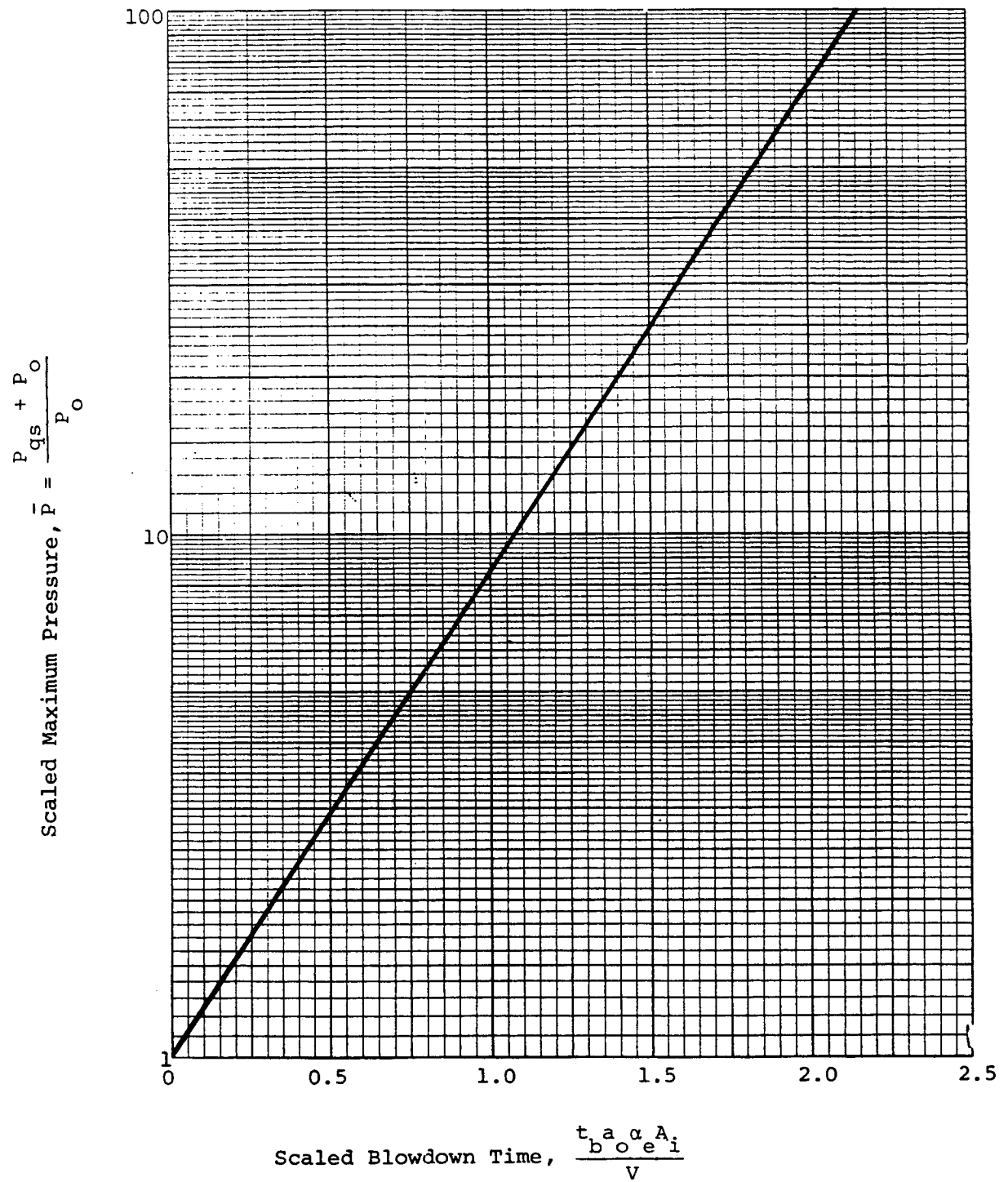


Figure 3-10. Scaled Blowdown Time Versus Scaled Maximum Pressure (Ref. 3-26)

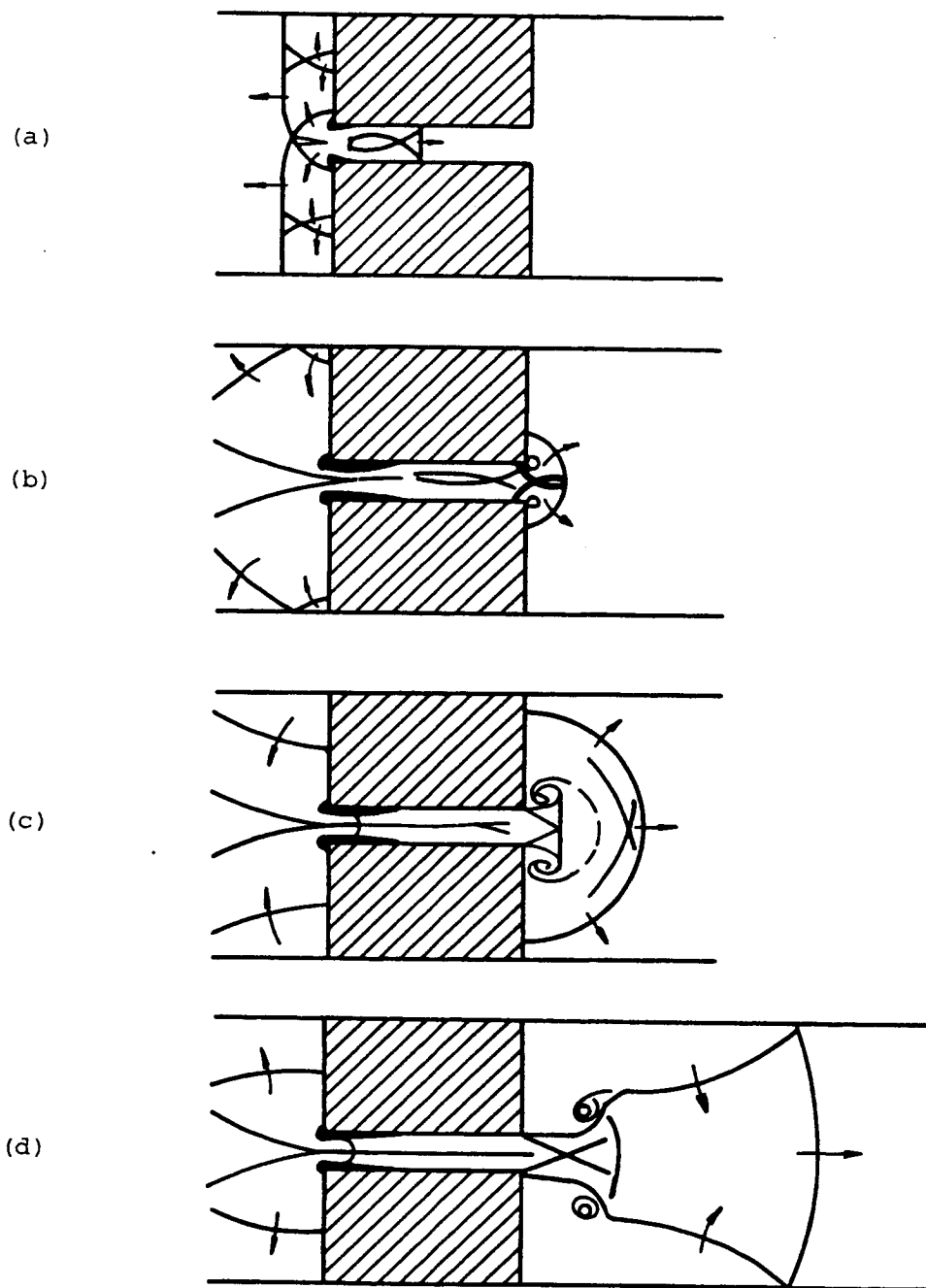


Figure 3-11. Stages During the Transmission of a Shock Wave Through a Single Slit in a Plate (Ref. 3-27)

becomes detached, and expands to fill the area behind the plate; see Fig. 3-11(d). The transmitted wave then reflects from the second layer and is again partially transmitted. This process continues for each layer until an attenuated shock emerges from the panel and reforms outside the structure. The detailed processes of reflection and transmission are very complex and result in multiple shocks. Even for transmission of a single shock through a single slit in a plate, the process is not simple, as can be seen in Fig. 3-11.

Various computer programs have been developed and used to attempt to predict intrapanel pressures and pressures transmitted through multi-layer panels. References 3-26 through 3-29 report intrapanel pressure predictions, and Ref. 3-30 reports predicted pressure transmission through an interlocked I-beam panel. Figure 3-12 illustrates typical results of the interlocked I-beam calculations of Ref. 3-30.

From the outset of suppressive structures testing and evaluation, measurements have been made of the characteristics of these external blast waves over a range of distances from the structures. References 3-21 and 3-31 through 3-36 contain the majority of such data. The following prediction methods presented are based upon these experimental data.

3.6.2 Prediction Methods

The prediction methods which follow have been developed by fitting curves to measured experimental data. They are strictly valid, therefore, only within the ranges of the variables for which measurements were obtained. Use of these expressions outside their range of applicability should be done only with extreme caution.

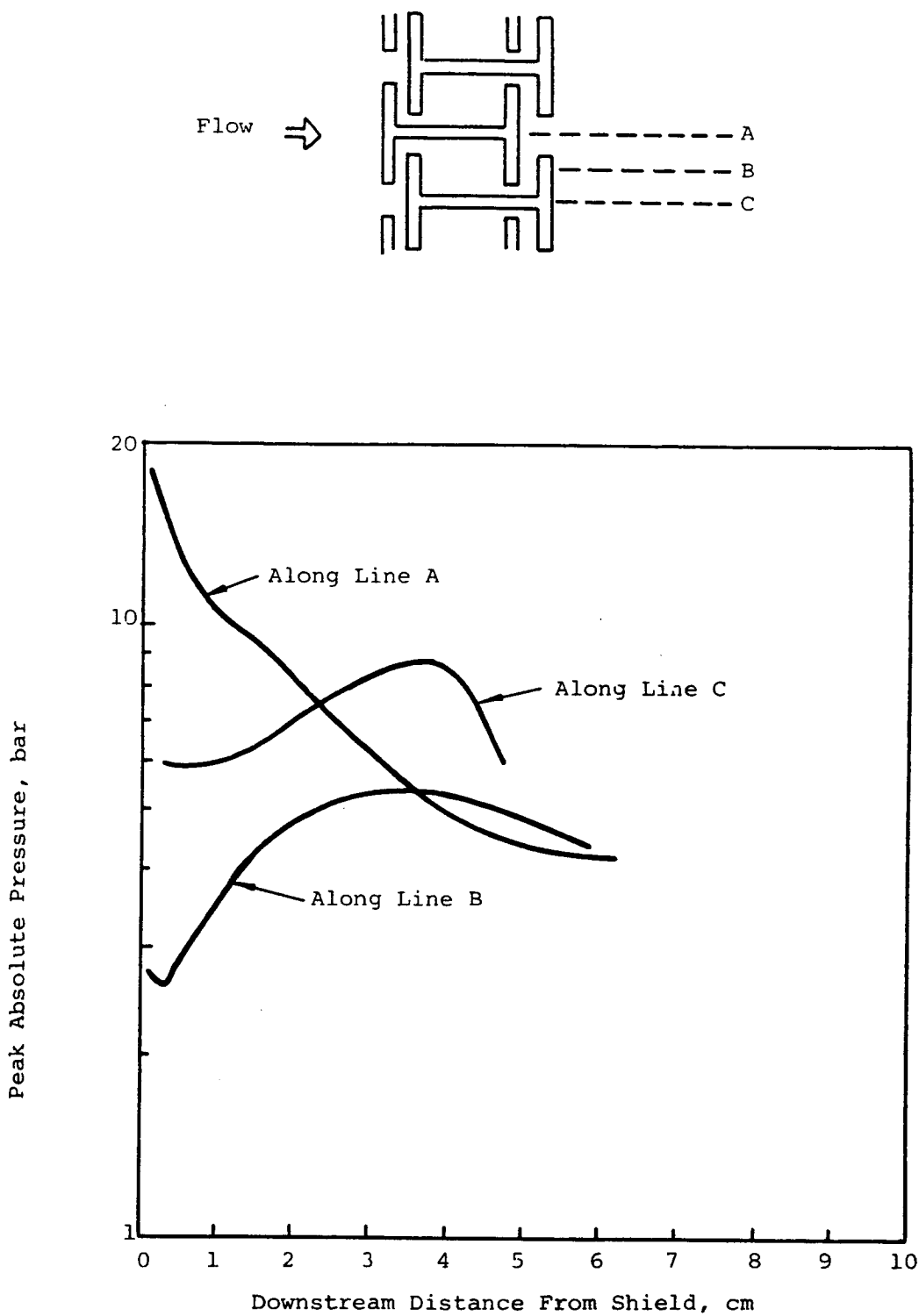


Figure 3-12. Calculated Pressures Outside Group 3 Cylindrical Blast Shield with 48-lb Charge (Ref. 3-30)

The expression for peak overpressure in psi outside a suppressive shield is (Ref. 3-19)

$$P_{so} = 957 \left(\frac{1}{Z} \right)^{1.66} \left(\frac{R}{X} \right)^{0.27} \left(\alpha_e \right)^{0.64} \quad (3-7)$$

where

Z = scaled distance, Eq. 3-2, pg. 3-6

R = distance from center of explosive charge to point of interest, ft

X = characteristic length of structure, ft;
side dimension for square structure; square root of plan area for rectangular structure; cube root of the volume for cylindrical structure

α_e = effective vent area ratio, Eq. 3-5, pg. 3-17

The limits for applicability of this equation are

$$2.93 \leq Z \leq 21.3$$

$$0.69 \leq R/X \leq 4.55$$

$$0.01 \leq \alpha_e \leq 0.13$$

and the expected error (standard deviation) is ± 19.9 percent.

The incident positive phase impulse in psi-ms outside a suppressive shield is given by (Ref. 3-19)

$$i_s = \left[218 \left(\frac{1}{Z} \right)^{0.98} \left(\frac{R}{X} \right)^{0.008} \left(\alpha_e \right)^{0.45} \right] W^{1/3} \quad (3-8)$$

where W is in pounds of TNT and the other terms are as previously defined. The limits of applicability of this equation are

$$2.93 \leq Z \leq 15.0$$

$$1.16 \leq R/X \leq 4.55$$

$$0.008 \leq \alpha_e \leq 0.13$$

and the expected error (standard deviation) is ± 19.2 percent. Additional equations are available for specific panel designs with smaller standard deviations (Ref. 3-19).

Equations 3-7 and 3-8 apply to any vented panel configuration which has been tested (e.g., all safety approved shields) and to uniformly vented structures, i.e., structures vented in the same manner through all sides and the roof.

3.7 FRAGMENTATION

3.7.1 Introduction

Fragments of interest in suppressive shielding may be classified as either primary or secondary. The term primary fragment denotes a fragment from an explosive-filled container which ruptures into many small pieces under detonation of the explosive material. Secondary fragments consist of objects which are located near an explosive source and are accelerated by the blast wave from the explosion. Secondary fragments may be initially restrained or fastened in some manner, or they may be unrestrained. Both types of fragments are discussed below.

a. Primary Fragments

Consider a cased high explosive charge such as a shell or missile warhead. The process of casing expansion and fracture on detonation of the explosive filler is well described in Ref. 3-37. The very high pressures generated by the detonating explosive cause the casing to expand to up to twice its original diameter. Radial cracks start on the outer surface of the casing but propagate only a short distance through the thickness. Failure is predominately in shear in the inner

part of the casing. Recovered fragments typically exhibit reductions in wall thickness of 40-60 percent according to Ref. 3-37.

The number and mass distribution of fragments formed during casing failure is a function of casing thickness, type of explosive, and metallurgy of the casing material. Natural fragments from cylindrical casings will often be portions of longitudinal strips and, consequently, will be rather long and slender. Numbers of fragments generated are usually quite large, typically in the thousands. Velocities of primary fragments are a function of the composition and geometry of the explosive charge and casing and the ratio of total explosive mass (or energy) to casing mass. Typically, primary fragment velocities from cased charges will be at least several thousand feet per second and can exceed seven thousand feet per second.

b. Secondary Fragments

Consider next the generation of secondary fragments. Loose or restrained objects located close to explosive sources can be accelerated by the strong blast waves from these sources and become potentially damaging fragments. In suppressive structures, these objects could be rollers on a conveyor line, motors and pieces of equipment used in munition plant operations, or a host of other items. Potential sources for secondary fragments can be determined from detailed study of specific plant operations and designs.

The initial reflected and diffracted blast waves accelerate the secondary fragments located close to the explosive source. Further from the source, both diffraction and drag forces can contribute to the acceleration. The mass and shape of potential secondary fragments can be estimated with a reasonable degree of certainty by inspection of the equipment and appurtenances at the hazardous location. Prediction of the velocity of secondary fragments is based upon impulse-momentum principles.

3.7.2 Prediction of Primary Fragmentation

Prediction of striking velocities of primary fragments for bursting munitions can be made with reasonable accuracy, but accurate prediction of mass and shape of these fragments for naturally fragmenting casings which do not employ pre-formed fragments is difficult. An unclassified expression for predicting primary fragment weight based upon Refs. 3-38 and 3-39 which has been partially verified by fragmentation tests using mild steel cylindrical casings filled with various explosives (Ref. 3-40) is

$$W_f = C \left[\ln \left(\frac{W_c}{2C} \right) \right]^2 \quad (3-9)$$

where

W_f = weight of the next to largest fragment, lb

$$C = \left[B t^{5/6} d_i^{1/3} (1 + t/d_i) \right]^2, \text{ lb}$$

B = constant depending upon type of explosive,
Table 3-2

t = thickness of casing, inches

d_i = inside diameter of casing, inches

W_c = weight of casing, lb

Prediction of primary fragment initial velocity can be accomplished with a semi-empirical procedure based upon the Gurney energy constant. The initial velocity of a primary fragment from a cylindrical metal case of uniform thickness filled with an evenly distributed explosive can be estimated with (Ref. 3-2)

$$v_o = \sqrt{2E'} \left[\frac{W/W_c}{1 + W/2W_c} \right]^{1/2} \quad (3-10)$$

Table 3-2

MOTT SCALING CONSTANTS FOR MILD STEEL CASINGS
AND VARIOUS EXPLOSIVES (Ref. 3-40)

Explosive	B (lb ^{1/2} inches ^{-7/6})
Baratol	0.128
Comp B	0.0554
Cyclotol (75/25)	0.0493
H-6	0.0690
HBX-1	0.0639
HBX-3	0.0808
Pentolite (50/50)	0.0620
PTX-1	0.0554
PTX-2	0.0568
TNT	0.0779
Comp A-3	0.0549
RDX/WAX (95/5)	0.0531
Tetryl	0.0681

where

v_o = initial primary fragment velocity, ft/sec

$\sqrt{2E'}$ = Gurney energy constant; Table 3-3

W = charge weight, lb

W_c = weight of the cylindrical portion of the metal casing, lb

Initial primary fragment velocities for other than cylindrical cross sectional shapes are shown in Table 3-4.

The primary fragment striking velocity, v_s , can be taken equal to the initial velocity for distances up to 20 feet from the detonation (Ref. 3-2). Since suppressive shield walls will typically be at or within this range, it is recommended that the fragment striking velocity be taken equal to the initial velocity for suppressive shielding applications.

3.7.3 Prediction of Secondary Fragmentation

The only expression presently available for estimating the initial velocity of secondary fragments is the semi-empirical relationship

$$v_{os} = \frac{A_p R_e g_s}{M} \left[0.556 \left(\frac{R_e}{R} \right) + 2.75 \left(\frac{R_e}{R} \right)^2 \right] \quad (3-11)$$

where

v_{os} = initial velocity of secondary fragment, in/sec

A_p = area of secondary fragment presented to explosive, in²

R_e = radius of spherical explosive charge, inches

M = mass of secondary fragment, lb-sec²/in

R = range from center of explosive charge to nearest face of secondary fragment, inches


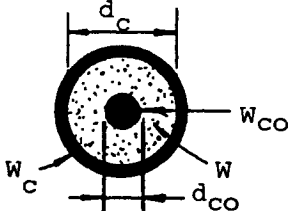
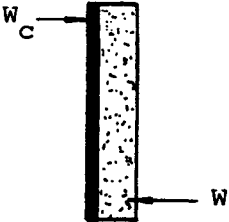
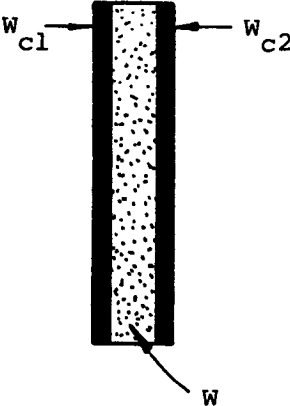
Table 3-3

GURNEY ENERGY CONSTANTS
FOR VARIOUS EXPLOSIVES (Ref. 3-41)

Explosive	$\sqrt{2E'}$ (ft/sec)
RDX	9,610
Comp C-3	8,790
TNT	7,780
Tritonal	7,610
Comp B	8,890
HMX	9,740
PBX-9404	9,510
Tetryl	8,200
TACOT	6,960
Nitromethane	7,910
PETN	9,610
Detasheet EL506D	7,480
Detasheet EL506L	7,220
Pentolite (50/50)	8,400

Table 3-4

INITIAL PRIMARY FRAGMENT VELOCITY
FOR VARIOUS CROSS-SECTIONAL SHAPES (Ref. 3-42 & 3-2)

Type	Cross Section	Initial Fragment Velocity
Sphere		$v_o = \sqrt{2E'} \left[\frac{W/W_c}{1 + 3W/5W_c} \right]^{1/2}$
Steel Cored Cylinder		$v_o = \sqrt{2E'} \left[\frac{W/W_c}{1 + \frac{(3+a)W}{6(1+a)W_c}} \right]^{1/2}$ <p>where $a = \frac{d_{co}}{d_c}$</p>
Plate		$v_o = \sqrt{2E'} \left[\frac{\frac{3W}{5W_c}}{1 + \frac{W}{5W_c} + \frac{4W_c}{5W}} \right]^{1/2}$
Sandwich Plates		<p>if $W_{c1} \neq W_{c2}$</p> $v_o = \sqrt{2E'} \left[\frac{W}{W_{c1} + W_{c2}g^2 + \frac{W}{3}(1-g+g^2)} \right]^{1/2}$ <p>where $g = \frac{W_{c1} + \frac{W}{2}}{W_{c2} + \frac{W}{2}}$</p> <p>if $W_{c1} = W_{c2} = W_c$</p> $v_o = \sqrt{2E'} \left[\frac{\frac{W}{2W_c}}{1 + \frac{W}{6W_c}} \right]^{1/2}$

$W, W_c, W_{cc}, W_{c1}, W_{c2}$ (lbs) d_c, d_{co} (inches) $v_o, \sqrt{2E'}$ (ft/sec)

g_s = secondary fragment shape factor
 = 2/3 for sphere
 = $\pi/4$ for side-on cylinder
 = 1 for end-on cylinder or plane surface

The limits of applicability of Eq. 3-11 are

$$1.5 \leq \frac{R}{R_e} \leq 6.0$$

$$0.18 \frac{\text{lb-sec}}{\text{in}^3} \leq \frac{Mv_o}{A_p R_e g_s} \leq 2.0 \frac{\text{lb-sec}}{\text{in}^3}$$

In addition to its rather narrow limits of validity, Eq. 3-11 is strictly applicable only to spherical charges of Comp B explosive and unrestrained secondary fragments of spherical or cylindrical shape. The speed calculated for an unconstrained secondary fragment represents an upper limit and, hence, conservative estimate of the speed of a constrained secondary fragment. Until further analytical and experimental work is completed, however, Eq. 3-11 is the best method available for predicting secondary fragment velocities.

3.8 IMPACT AND PENETRATION

3.8 Introduction

The accidental detonation in an explosive processing plant can result in the generation of many primary and/or secondary fragments. On contact with a suppressive shield, the fragment will either penetrate some distance into the structure and be stopped, or perforate completely through and emerge from the back face with some residual velocity and mass. Whether partial penetration or perforation occurs depends on a variety of parameters including the thickness, construction details and material properties of the barrier; the geometry and material

characteristics of the fragment, fragment mass, presented area, striking velocity and angle at which the fragment strikes the wall. Several characteristic mechanisms for penetration that have been observed in steel plates are illustrated in Fig. 3-13. Plugs are most likely to be found in very hard plates of moderate thickness, while petalling is most frequently observed in thin plates struck at or below ordnance velocities (2500 fps). A combination of ductile failure and spalling is characteristic for perforation of thick plates of medium or low hardness.

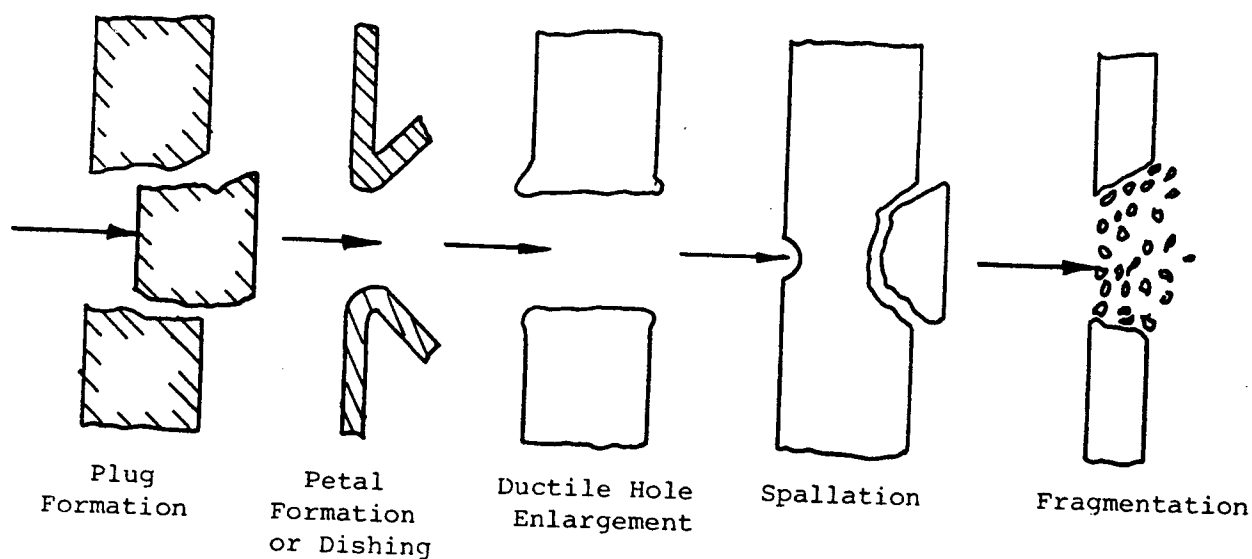


Figure 3-13. Possible Mechanisms for Steel Plate Damage

Three possible mechanisms of fragment impact damage of concrete panels are shown in Fig. 3-14. At low velocities, the fragment strikes the panel and rebounds without causing any local damage. As the velocity increases, pieces of concrete are spalled off of the front face of the target. This spalling forms a spall crater that extends over a substantially greater area than the cross sectional area of the striking fragment. As the velocity continues to increase, the fragment will penetrate the target to depths beyond the depth of the spall crater,

forming a cylindrical penetration hole with a diameter only slightly greater than the fragment diameter. Further increases in velocity produce cracking of the concrete on the back surface followed by scabbing of concrete from this rear surface. The zone of scabbing will generally be much wider, but not as deep as the front face spall crater. Once scabbing begins, the depth of penetration will increase rapidly. As the fragment velocity increases further, perforation of the target will occur as the penetration hole extends through to the scabbing crater. Still higher velocities will cause the missile to exit from the rear face of the target.

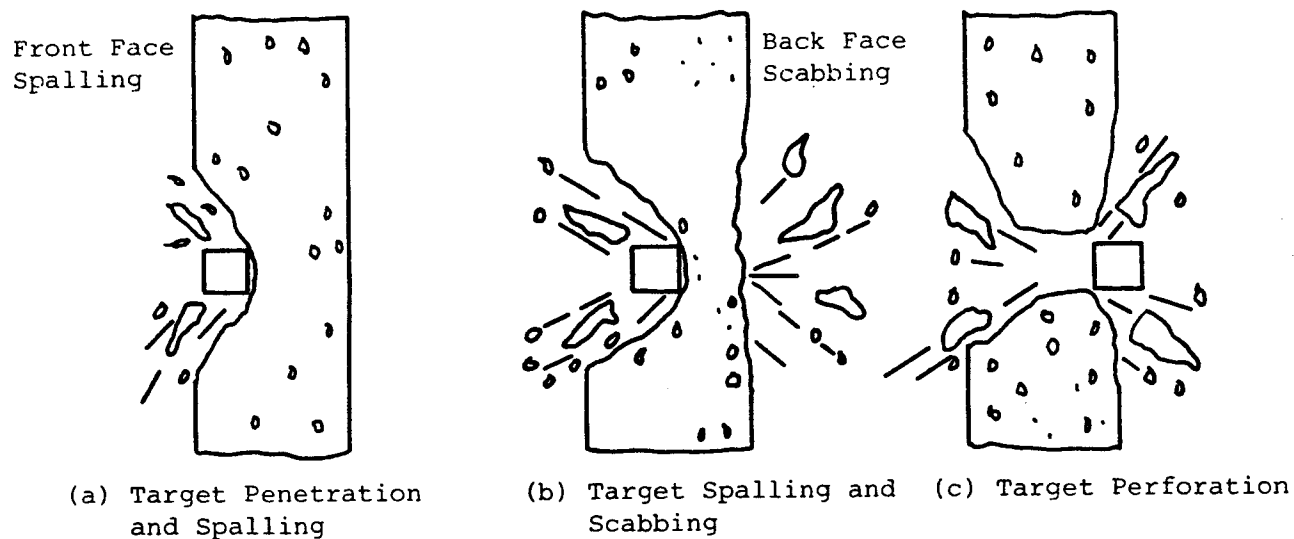


Figure 3-14. Possible Mechanisms for Concrete Panel Impact Damage (Ref. 3-43)

3.8.2 Prediction of Penetration of Steel Plate

The recommended method for predicting fragment penetration of steel plate(s) is based on the procedures of Ref. 3-44 and is shown in outline form in Fig. 3-15. The prediction method and quantities required for its utilization are discussed further below.

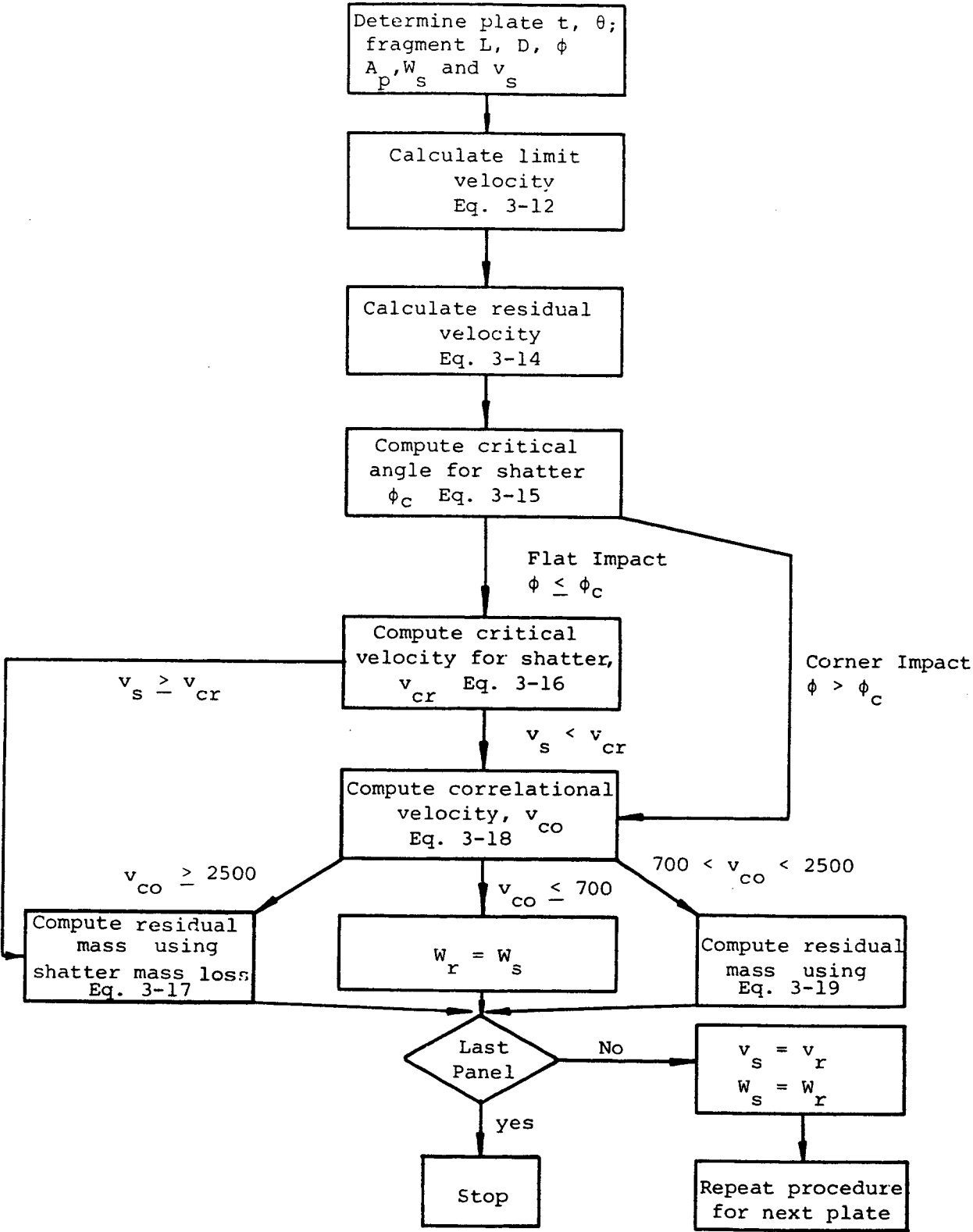


Figure 3-15. Prediction of Fragment Penetration of Steel Plate

a. Input Parameters

Quantities needed to begin the procedure are

- Plate thickness, t inches
- Angle of obliquity = angle between line of flight of fragment and the normal to the plate surface, θ degrees
- Orientation angle = least angle between any flat fragment surface and the plate surface, ϕ degrees
- Fragment length to diameter ratio, L/D
- Fragment area presented to plate, A_p in²
- Fragment striking weight, W_s lb
- Fragment striking velocity, v_s fps

These quantities will either be known or can be estimated for the problem of interest. Otherwise, they must be assumed.

b. Ballistic Limit Velocity

The ballistic limit velocity is defined as the lowest striking velocity that results in perforation of the target with zero residual velocity. The ballistic limit velocity for compact fragments striking mild steel targets can be estimated as

$$v_\ell = \frac{A_o}{\sqrt{W_s}} A_p^m (t \sec \theta)^n \quad (3-12)$$

where v_ℓ is the ballistic limit velocity in fps; A_o , m and n are constants defined in Table 3-5; and the other terms are as previously defined.

Equation 3-12 is also applicable to perforated plates with the substitution of $R^2 A_p$ for A_p , where R is the perforation factor. The perforation factor is defined as

Table 3-5

EMPIRICAL CONSTANTS FOR PREDICTING COMPACT FRAGMENT
LIMIT VELOCITY FOR MILD STEEL TARGETS
(Southwest Research Institute)

L/D	$\frac{t}{R/\bar{A}_p} *$	A_o	m	n
≤ 5	$0 \leq 0.46$	1414	0.295	0.910
≤ 5	$0.46 \leq 1.06$	1936	0.096	1.310
≤ 5	≥ 1.06	2039	0.064	0.430
> 5	-	1261	0.427	0.647

* R is the perforation factor for perforated plates;
see Eq. 3-13 or Fig. 3-16.

Table 3-6

EMPIRICAL CONSTANTS FOR PREDICTING COMPACT FRAGMENT
RESIDUAL VELOCITY FOR MILD STEEL TARGETS

Constant	L/D < 5	L/D \geq 5
a	1.12	1.10
b	0.52	0.80
c	1.29	1.45

(Southwest Research Institute)

$$R = 1 - d_p/h_p \quad (3-13)$$

where d_p is the diameter of the perforations and h_p is the average center-to-center distance between perforations. Values of the perforation factor as a function of vent area ratio, α , for hexagonal and square hole patterns are shown in Fig. 3-16.

c. Residual Velocity

In order to predict the residual velocity of a fragment that has perforated a mild steel plate, a quantity

$$x = \frac{v_s}{v_\ell} - 1$$

is computed first where v_s is the striking velocity and v_ℓ the ballistic limit velocity. Then,

$$v_r = v_\ell \beta \left[\frac{ax^2 + bx + c\sqrt{x}}{x + 1} \right] \quad (3-14)$$

$$\text{but } v_r \leq v_s$$

where

$$\beta = \frac{1}{\left[1 + \gamma A_p t / W_s \right]^{1/2}} \quad \text{for } L/D \leq 2$$

$$\beta = 1 \text{ for } L/D > 2$$

$$\gamma = \text{density of the target plate, lb/in}^3 \text{ (should take account of holes for perforated plates)}$$

$$a, b, c = \text{constants from Table 3-6}$$

d. Critical Angle for Shatter

A fragment which has perforated a mild steel plate may or may not lose mass depending upon the orientation angle ϕ between any flat fragment face and the target. If ϕ is small enough, the impact is essentially flat, or $\phi \leq \phi_c$, where ϕ_c is the critical orientation angle in degrees for shatter.

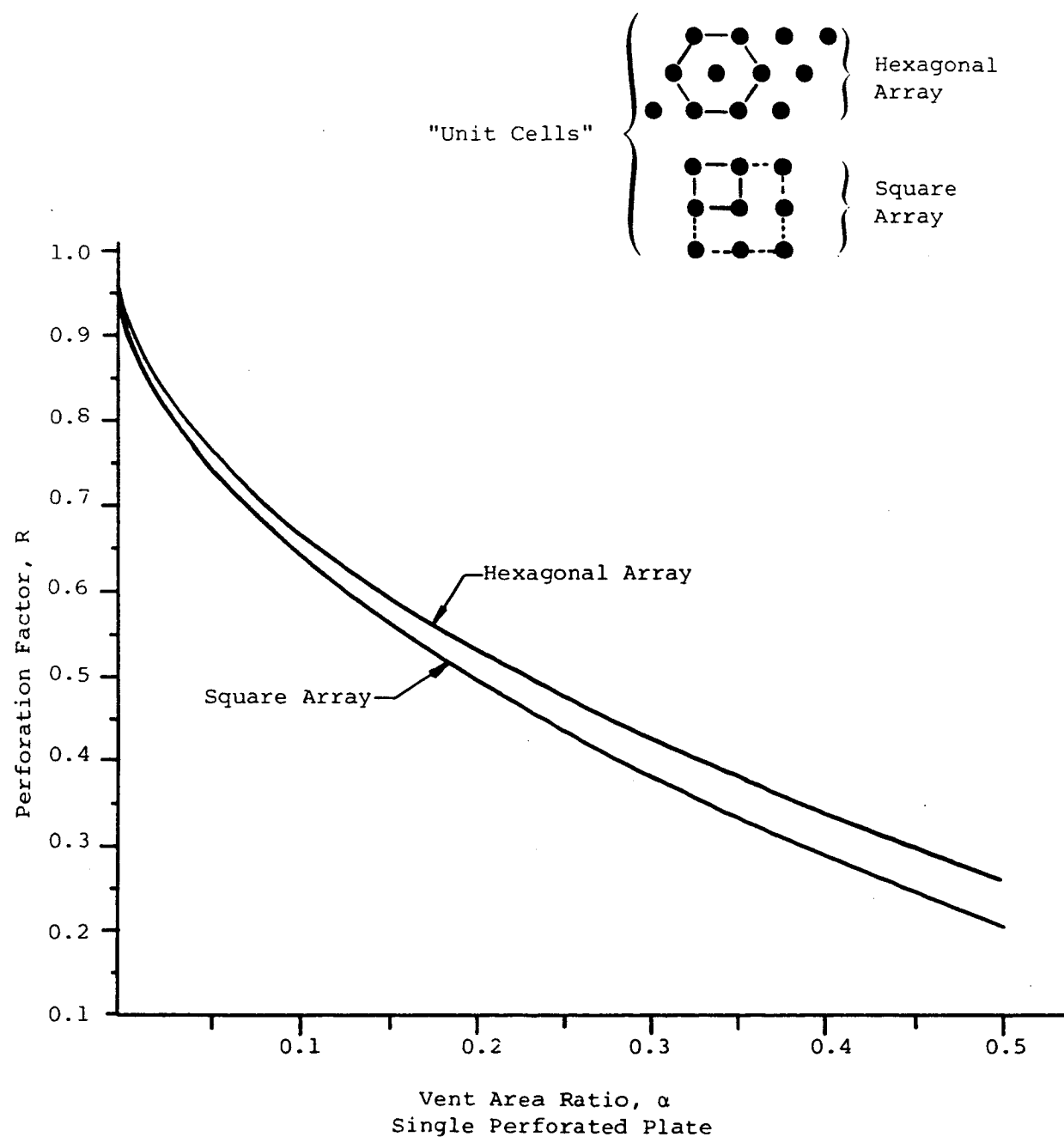


Figure 3-16. Perforation Factor Versus Vent Area Ratio for Drilled Hole Patterns
(Southwest Research Institute)

$$\phi_c = \arcsin(v_s \cos \theta / c_p) \quad (3-15)$$

where c_p = sonic velocity of the plate = 18,010 fps for steel. If $\phi > \phi_c$, the impact is considered to be a corner or edge impact.

Define a critical velocity as

$$v_{cr} = 2000 \text{ fps} / \cos \theta \quad (3-16)$$

Then, for a flat impact with a striking velocity equal to or greater than the critical velocity, i.e.,

$$\phi \leq \phi_c$$

$$v_s \geq v_{cr}$$

the fragment will be in the shatter mass loss mode. The residual weight of the fragment for this case is determined by

$$W_r = W_s \left[1 - 0.002063 t^{0.138} W_s^{0.074} (\sec \theta)^{0.143} v_s^{0.761} \right] \quad (3-17)$$

where all terms are as previously defined.

For flat impacts with a striking velocity less than the critical velocity, i.e.,

$$\phi \leq \phi_c$$

$$v_s < v_{cr}$$

and for all corner or edge impacts, i.e.,

$$\phi > \phi_c$$

the fragment is in the deformation mass loss mode. To determine the fragment residual mass for this mode, a correlation velocity is computed first. The correlation velocity in fps is defined as

$$v_{co} = \frac{v_s}{1 + \frac{\frac{0.6t\gamma A_p}{W_s} \cos\theta}{+ 0.15}} \quad (3-18)$$

where all terms are as previously defined. Then,

$$\text{For } v_{co} \leq 700 \text{ fps: } W_r = W_s$$

$$v_{co} \geq 2500 \text{ fps: } W_r = \text{Eq. 3-17}$$

$$700 \text{ fps} < v_{co} < 2500 \text{ fps:}$$

$$W_r = W_s \left[1 - 0.0000151(v_{co} - 700)^{1.42} \right] \quad (3-19)$$

The penetration prediction method outlined above can be expected to give conservative results, particularly for fragment residual mass estimates. Two further assumptions can be made when investigating multi-layer panels that will increase the conservatism of the method and reduce the number of calculations required. These are (1) to set $\beta = 1$ in Eq. 3-14, and (2) to neglect any fragment loss of mass. If the panel defeats the fragment with the resulting known higher residual velocity and larger mass, it is clearly safe. If the fragment defeats the panel with these two assumptions, the calculations can be repeated with the more realistic fragment residual velocity and mass.

3.8.3 Prediction of Penetration of Concrete Panels

For a very quick and crude rule-of-thumb estimate of the effectiveness of reinforced concrete panels in resisting penetration by steel fragments, it can be assumed that one inch of mild steel is equivalent to nine inches of concrete, i.e., if it is known that a one-inch thickness of mild steel will defeat a particular fragment threat, it can be estimated that nine inches of reasonable quality reinforced concrete will also defeat the fragment. When more realistic estimates of concrete

penetration are desired, the methods from Ref. 3-2 summarized below can be utilized.

a. Armor-Piercing Fragments

A certain amount of experimental data analogous to primary fragment penetration has been accumulated in connection with projects to determine the effects of bomb and projectile impact on concrete structures. These data were analyzed and relationships developed where the amount of fragment penetration into concrete elements could be expressed in terms of the physical properties of both the metal fragment and the concrete. The general expression for the maximum penetration X_f in inches of a compact armor-piercing fragment was derived in terms of the fragment weight W_{fo} in ounces and striking velocity v_s in fps, i.e.,

$$X_f = 1.62 \times 10^{-5} W_{fo}^{0.4} v_s^{1.8} \quad (3-20)$$

Equation 3-20 is based on a concrete compression strength f'_c equal to 5,000 psi. Maximum penetrations of fragments in concrete of other strengths may be obtained by multiplying the value of X_f of Eq. 3-20 by the square root of the ratio of 5,000 psi to the compressive strength of the concrete in question. Figure 3-17 is a plot of the maximum penetration through 5,000 psi concrete for various fragment sizes and striking velocities.

The limiting thickness of concrete at which perforation will occur can be obtained from Fig. 3-18 and is a function of the coefficient C_1 , the fragment weight, striking velocity, and maximum penetration and the dilatational velocity c_s of the elastic wave through concrete where

$$c_s = 5.16 E_c^{1/2} \text{ (ft/sec)} \quad (3-21)$$

and the modulus of elasticity E_c is defined to be